Geochemistry, Geophysics, Geosystems

RESEARCH ARTICLE
10.1029/2019GC008751

Alkenone Distributions and Hydrogen Isotope Ratios Show Changes in Haptophyte Species and Source Water in the Holocene Baltic Sea

Gabriella M. Weiss[1,2], Barbara Massalska[1,3], Rick Hennekam[4], Gert-Jan Reichart[4,5], Jaap S. Sinninghe Damsté[1,5], Stefan Schouten[1,5], and Marcel T. J. van der Meer[1]

[1]Department of Marine Microbiology and Biogeochemistry, NIOZ Royal Netherlands Institute for Sea Research and Utrecht University, Texel, The Netherlands, [2]Now at Department of Geosciences, Pennsylvania State University & Division of Geological and Planetary Sciences, California Institute of Technology, Pasadena, CA, USA, [3]Department of Geology, University of Warsaw, Warsaw, Poland, [4]Department of Ocean Systems, NIOZ Royal Netherlands Institute for Sea Research and Utrecht University, Texel, The Netherlands, [5]Department of Earth Sciences, Faculty of Geosciences, Utrecht University, Utrecht, The Netherlands

Key Points:
- Unusual alkenone isomers are reported for Holocene sediments from the Arkona Basin, Baltic Sea
- Hydrogen isotope ratios of alkenones correspond to changes in source water as well as changes in species and salinity
- Alkenone distributions show mixing of different haptophyte groups, which changed with well-established Baltic Sea phase shifts

Supporting Information:
- Supporting Information S1

Correspondence to:
G. M. Weiss, gabriella.weiss@nioz.nl

Citation:
Weiss, G. M., Massalska, B., Hennekam, R., Reichart, G.-J., Sinninghe Damsté, J. S., Schouten, S., & van der Meer, M. T. J. (2020). Alkenone distributions and hydrogen isotope ratios show changes in haptophyte species and source water in the Holocene Baltic Sea. *Geochemistry, Geophysics, Geosystems*, *21*, e2019GC008751. https://doi.org/10.1029/2019GC008751

Received 10 OCT 2019
Accepted 17 JAN 2020
Accepted article online 08 FEB 2020

Abstract The Baltic Sea, a dynamic, marginal marine basin, experienced a number of large changes in salinity during the Holocene as a result of fluctuations in global and local sea level related to melting of glacial ice sheets and subsequent isostatic rebound. These changes likely had pronounced effects on the species composition of haptophytes, a common phytoplankton group found in the Baltic Sea. This dynamic environment provides the ideal setting to study how species change impacts distribution and hydrogen isotope ratios of long-chain alkenones (δ^2H_{C37}), haptophyte-specific biomarkers. Here we analyzed the aforementioned parameters in Holocene sediments covering the contrasting hydrological phases of the Baltic Sea. Alkenone distributions changed with different Baltic Sea salinity phases, suggesting that species shifts coincide with salinity change. δ^2H_{C37} values show two major shifts: one in the middle of the freshwater Ancylus Lake phase (10.6 to 7.7 ka) and a second at the transition from the brackish Littorina Sea phase (7.2 to 3 ka) into the fresher Modern Baltic (3 ka to the present). The first shift represents a significant enrichment of 50‰, which cannot be explained by salinity or species changes only. At this time, the isotopically depleted ice sheets had melted, and only the relatively enriched freshwater source remained. The second shift, coincident with a change in distribution, is likely caused by a change in species composition alone. These findings show that hydrogen isotope ratios of long-chain alkenones, combined with their relative distribution, can be used to reconstruct changes in source water.

Plain Language Summary Algae record information about the water they grow in, for example, if the water is from the ocean or freshwater sources. This information is preserved in organic compounds and can be elucidated by measuring the stable hydrogen isotope composition of these molecules. The Baltic Sea is particularly suited to study hydrological changes preserved in organic compounds because it maintains a connection with the North Sea, encompassing a range of ocean to freshwater habitats, and this connection has fluctuated over time causing large salinity changes. We investigated hydrological changes in the Baltic Sea over the last 11,000 years. In the older part of the record, a major shift in isotopes of algal compounds occurred without a shift in the algal population. We interpret this as the melting of the last remnants of glacial-aged ice at this time, leading to an abrupt shift to other freshwater sources. In the younger parts of the record, more ocean water entered the Baltic Sea, causing a change in the algal population along with isotopic change. Overall, these results contribute to our knowledge of how water source and salinity affect algal populations, which is important for understanding how ecosystems might respond to future climate change and hydrological budget.

1. Introduction

Haptophyte algae are important primary producers and believed to be one of the most substantial producers of calcium carbonate globally (Laguna et al., 2001; Paasche, 2002) inhabiting both lacustrine and marine environments (Theroux et al., 2010). Haptophytes are extremely diverse, with over 300 documented species (Jordan & Chamberlain, 1997). Certain species of the order Isochrysidales are the only known producers of long-chain alkenones and polyunsaturated methyl and ethyl ketones with chain lengths between 35 and 42

carbon atoms (de Leeuw et al., 1980; Volkman et al., 1980; Theroux et al., 2010; Araie et al., 2018). These long-chain alkenones are often well preserved in sediments and provide highly useful proxies to understand past changes in global climate, in particular the $U^{K'}_{37}$ index, a proxy for sea surface temperature (Brassell et al., 1986; Müller et al., 1998; Prahl & Wakeham, 1987; Tierney & Tingley, 2018). Furthermore, the hydrogen isotope composition of long-chain alkenones (δ^2H_{C37}) has been shown to strongly relate to salinity and the δ^2H values of water (e.g., Chivall et al., 2014a; M'Boule et al., 2014; Sachs et al., 2016; Schouten et al., 2006; Weiss et al., 2017), which has led to the use of δ^2H_{C37} values to reconstruct paleosalinity in a number of different marine environments (Pahnke et al., 2007; van der Meer et al., 2007, 2008; Leduc et al., 2013; Kasper et al., 2014, 2015; Petrick et al., 2015; Simon et al., 2015; Weiss, de Bar, et al., 2019). However, other factors such as growth rate (Sachs & Kawka, 2015), growth phase (Chivall et al., 2014a; Wolhowe et al., 2009), and light intensity (van der Meer et al., 2015; Weiss et al., 2017) are also known to affect the δ^2H values of alkenones. While the latter factors exhibit significant controls on δ^2H values in culture, environmental studies do not always reflect these effects and often salinity variations appear to be the strongest signals (Weiss, Schouten, Sinninghe Damsté, & van der Meer, 2019, and references therein).

One particular factor that is not well constrained yet is the impact of species composition on the δ^2H values of alkenones. It has been noted that species fractionate hydrogen differently relative to each other, resulting in ^2H enrichment of alkenones produced by marginal marine species relative to δ^2H values of alkenones from marine species (Schwab & Sachs, 2011; M'Boule et al., 2014; Nelson & Sachs, 2014; Weiss, Schouten, et al., 2019). Alkenone-producing haptophytes are separated into three distinct groups based on 18S ribosomal RNA (Theroux et al., 2010), and each group seems to prefer niches with a distinct salinity range. Group I haptophytes are presently uncultured but have been found in freshwater, lacustrine environments in the Northern Hemisphere (Theroux et al., 2010; Longo et al., 2016, 2018; Plancq, Cavazzin, et al., 2018; Plancq, McColl, et al., 2018). Group II haptophytes are the most cosmopolitan, found in both oligohaline and hypersaline lakes (Longo et al., 2016; Theroux et al., 2010), and cultured representatives include *Isochrysis galbana* and *Ruttnera lamellosa*. Marine species fall under Group III haptophytes, which include *Emiliania huxleyi* and *Gephyrocapsa oceanica* (Theroux et al., 2010). Only recently, analytical advances have allowed for better constraint on the contributions of each of these three groups to the pool of sedimentary alkenones. Groups can now be distinguished because of improved separation that allows for detection of tri-unsaturated alkenone positional isomers with different double bond positions at $\Delta^{14,21,28}$ instead of the common $\Delta^{7,14,21}$ configuration (Dillon et al., 2016; Longo et al., 2013, 2016). These so-called "tri-unsaturated isomers" have been detected alongside the traditional $C_{37:3}$ methyl, $C_{38:3}$ ethyl and methyl, and $C_{39:3}$ ethyl alkenones and allow for better distinction between haptophyte groups. Each haptophyte group appears to have different alkenone distributions: Group I is characterized by the presence of the novel tri-unsaturated isomers of C_{37}-C_{39}, in addition to the regular di-, tri- and tetra-unsaturated C_{37}-C_{39} alkenones; Group II does not synthesize the novel tri-unsaturated isomers and rarely produces C_{38} methyl alkenones but instead synthesizes the standard suite of C_{37}-C_{39} and is also thought to produce the shorter chain C_{35} and C_{36} alkenones. The latter alkenones have been detected in marginal marine environments generally characterized by having low salinities compared to the open ocean (Rontani et al., 2001; Xu et al., 2001; Fujine et al., 2006; van Soelen et al., 2014; Warden et al., 2016; Weiss, Schouten, et al., 2019). These shorter chain alkenones have also appeared in an *E. huxleyi* culture after being kept in cultivation for a few years (Prahl et al., 2006). In contrast to the C_{37}-C_{40} alkenones, the C_{35} and C_{36} are thought to be synthesized from the $C_{37:2}$ and $C_{38:2}$, respectively, via β-oxidation and produced by mutants of Group II species in the natural environment (Zheng, Dillon, et al., 2016; Zheng, Huang, et al., 2016). Finally, Group III produce the standard suite of C_{37} methyl and C_{38} ethyl and methyl alkenones, with low abundance of the C_{39} ethyl alkenones in some cases (Longo et al., 2013). All three groups are known to live in the Baltic Sea (Kaiser et al., 2019) providing the perfect opportunity to determine how distribution changes can enhance our understanding of shifts in alkenone producers when environments experience large fluctuations in salinity.

Besides different alkenone distributions, the hydrogen isotope ratios of long-chain alkenones also differ by group; more depleted δ^2H_{C37} values are noted for Group III haptophytes compared to Group II when both are grown at the same salinity (Chivall et al., 2014a; M'Boule et al., 2014). Based on distributions and hydrogen isotope ratios of alkenones, mixed contributions of Groups I and II as well as Groups II and III have been noted in some environments (Schwab & Sachs, 2011; Nelson & Sachs, 2014; Weiss, Schouten, et al., 2019), but a mixing of all three groups based on distributions has only been observed for surface sediments of

the Baltic Sea (Kaiser et al., 2019). In that case, a transect from the Kattegat into the Baltic Sea basin showed the presence of all three haptophyte groups reflected in changing alkenone distributions. This was confirmed by 18S rDNA preserved in surface sediments (Kaiser et al., 2019). Additionally, the relative percent contribution of the $C_{37:4}$ alkenone ($\%C_{37:4}$) increases for Group II species (Chivall et al., 2014b) and has been proposed as a salinity proxy in culture and modern Baltic Sea sediments (Kaiser et al., 2017).

The findings of Kaiser et al. (2019) have potentially large consequences for interpreting the sedimentary record of the Baltic Sea with respect to δ^2H_{C37} composition, as the Baltic Sea experienced varying salinities throughout the Holocene. The Baltic Sea began as the freshwater Baltic Ice Lake at around 13 ka BP and transitioned into a brackish basin known as the Yoldia Sea (from 11.6 to 10.6 ka BP; Moros et al., 2002) as deglaciation led to rising sea levels (Mörner, 1995). Continental uplift as a result of the isostatic adjustment to the melting of the Scandinavian Ice Sheet closed off the Baltic Sea from the North Sea, giving rise to the Ancylus Lake phase noted for having surface waters that were fresh (from 10.6 until approximately 7.7 ka BP; Moros et al., 2002). This freshwater phase ended when a large marine transgression brought North Sea water into the basin, shifting the Baltic Sea into the brackish Littorina Sea phase (Moros et al., 2002). The Littorina Sea lasted for a few thousand years, from 7.2 to around 3 ka BP with a gradual freshening into the Modern Baltic phase as a consequence of continued continental uplift, which was mainly noted in the Baltic proper (Andrén et al., 2000; Björck, 1995). Initial work on a Holocene sediment core has shown that hydrogen isotope ratios of long-chain alkenones from the Baltic Sea might reflect changes in species composition (Warden et al., 2016), but techniques used in that study did not allow for detection of tri-unsaturated isomers and alkenones of lower abundance; thus, no detailed reconstructions of species changes could be made.

Here we generated a comprehensive down-core record of δ^2H_{C37} values and alkenone distributions from the Arkona Basin in the Baltic Sea analyzed on an RTX-200 60 m GC column, allowing for the separation and detection of individual alkenones and isomers. Detection of these isomers allowed for changes in species composition to be determined based on alkenone distributions which were related to the different Baltic Sea phase shifts. The Arkona Basin also provided an ideal setting for testing how well hydrogen isotope ratios of long-chain alkenones are recording salinity changes in marginal marine environments and how isotopic change relates to species shifts.

2. Materials and Methods

2.1. Location and Climate History

A 12 m piston core (64PE410-S7) was recovered from the Arkona Basin of the Baltic Sea (54°50.910′N, 13° 21.412′E) with RV Pelagia in May 2016. The Arkona Basin is located in the western edge of the Baltic Sea next to the open connection with the North Sea via the Kattegat and Skagerrak (Figure 1). Situated at the western edge of the Baltic Sea, the Arkona Basin is perfectly suited for finding evidence of major marine transgressions and regressions occurring throughout the Baltic Sea climate history. The Arkona Basin has slightly higher salinities at present (~8 g kg^{-1}) compared to the Baltic proper as a result of an open connection with the Kattegat. The phases in the development of the Baltic Sea during the Holocene are relatively well established (Björck, 1995), but the timing of these events in the Arkona Basin differs somewhat from timing reported for the Baltic proper, specifically the timing of the marine transgression that ended the Ancylus Lake phase (Warden et al., 2016). Around ~7.7 ka, a large marine transgression occurred, bringing saline water into the basin and permanently restoring the connection to the North Sea (Moros et al., 2002; Warden et al., 2016).

2.2. Long-Chain Alkenones

Samples for long-chain alkenone analyses were taken every ~100 cm in the top section of the core and then every 10 cm between 930 cm and the bottom (1,216 cm). In total, 41 sediment samples were freeze dried, and organics were extracted using a Dionex Accelerated Solvent Extractor. Following Accelerated Solvent Extractor, total lipid extracts were collected and separated into three fractions using small aluminum oxide columns. An apolar fraction was separated using hexane:dichloromethane 9:1 (*v*:*v*), a ketone fraction using hexane:dichloromethane 1:1 (*v*:*v*), and a polar fraction using dichloromethane: methanol 1:1 (*v*:*v*). Following separation over an aluminum oxide column, alkenones ended up in the

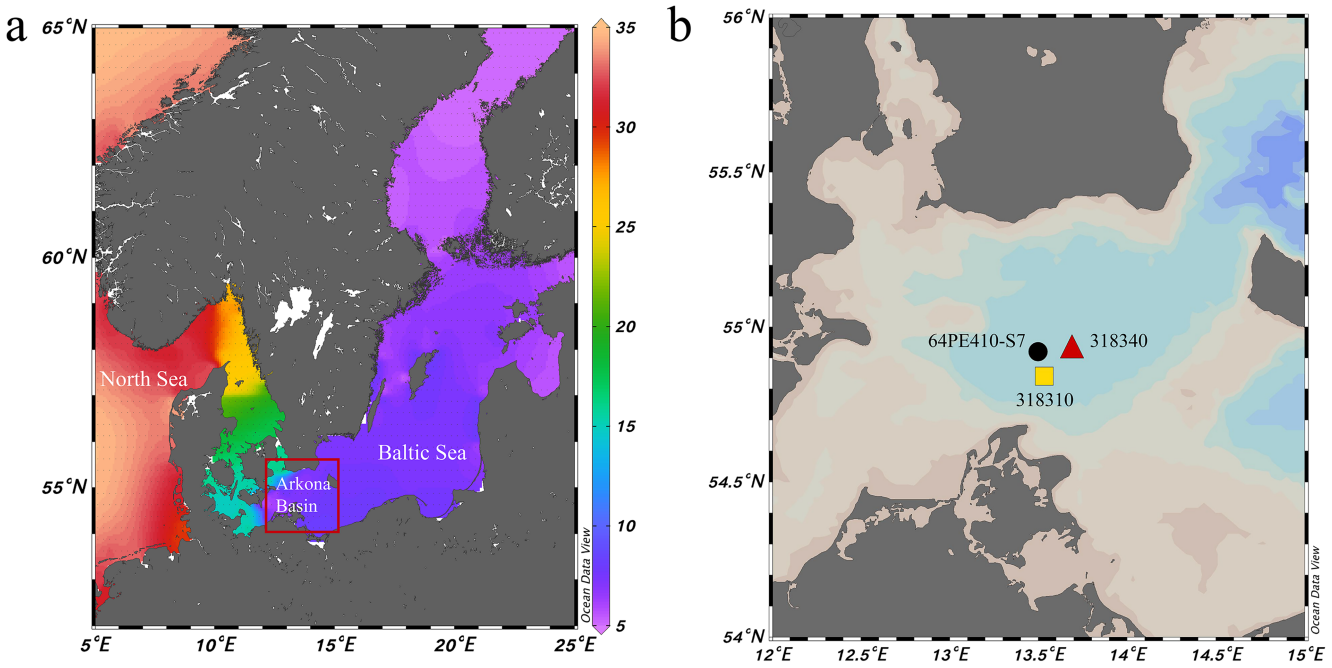

Figure 1. (a) Map showing annual mean salinity from the World Ocean Atlas 13 (Zweng et al., 2013) for the North Sea into the Baltic Sea. The Arkona Basin is noted by the red box. (b) The location (54°50.910′N, 13°21.412′E) of Core 64PE410-S7 (black circle) in the Arkona Basin of the Baltic Sea. The age model for 64PE410-S7 is based on radiocarbon dating and comparison with two well-dated neighboring cores, 318310 (54°50.34′N, 13°32.03′E) and 318340 (54°55.77′N, 13° 41.44′E), noted by the yellow square and red triangle, respectively, from Warden et al. (2016).

ketone fraction and were cleaned over a silver nitrate impregnated silica gel column using 100% dichloromethane to remove coeluting compounds, and alkenones were eluted using dichloromethane: ethyl acetate 1:1 (*v*:*v*). Alkenone concentrations were determined by using a gas chromatograph with a flame ionization detector equipped with an RTX-200 column (Restek, 60 m × 0.32 mm × 0.5 μm) and quantified based on a known concentration of a C_{19} ketone internal standard (supporting information Table S1). Alkenones were identified using a gas chromatograph coupled to a mass spectrometer equipped with the same 60 m RTX-200 column. The GC temperature program was as follows: 70 to 250 °C at 18 °C/min, 250–320 °C at 1.5 °C/min, and then kept at 320 °C for 25 min at a flow rate of 1.5 ml/min. Two indices have been proposed to trace the presence of Group I haptophytes (Longo et al., 2016):

$$RIK_{37} = \frac{C_{37:3a}}{C_{37:3a} + C_{37:3b}}, \tag{1}$$

$$RIK_{38E} = \frac{C_{38:3a}\,Et}{C_{38:3a}\,Et + C_{38:3b}\,Et}. \tag{2}$$

In these equations, "a" represents the traditional $C_{37:3}$ and $C_{38:3}$ alkenones, and "b" represents the novel tri-unsaturated isomers. These indices, along with the binary mixing model from Longo et al. (2018)

$$\%\text{Group II} = \frac{RIK_{37} - 0.56}{0.44}, \tag{3}$$

were used to determine the percentage of Group I and Group II haptophytes in samples containing tri-unsaturated isomers. When Group I species were present, temperature was calculated using R3b index:

$$R3b = \frac{C_{37:3b}}{C_{38:3b}\,Et + C_{37:3b}}, \tag{4}$$

and subsequent temperature calibration from Longo et al. (2018):

$$T = \frac{R3b - 0.42}{0.032}. \quad (5)$$

Salinity was calculated using the $\%C_{37:4}$ calibration from Kaiser et al. (2017):

$$\%C_{37:4} = -5.8353\, x\, S + 51.8028, \quad (6)$$

with $\%_{C37:4}$ being the concentration of $C_{37:4}$ as a percentage of total C_{37} alkenones. Furthermore, salinity was estimated from the RIK_{37} salinity calibration from Kaiser et al. (2019):

$$S = \frac{RIK_{37} + 0.5319}{0.0677}. \quad (7)$$

2.3. Hydrogen Isotope Analyses

Hydrogen isotope ratios of alkenones were measured using gas chromatography coupled to an isotope ratio mass spectrometer via a high temperature conversion reactor. The GC was also equipped with an RTX-200 60 m column using the temperature program described in Weiss, Schouten, et al. (2019). At the start of each day, the H_3^+ factor was calculated and corrected for, which ranged from 2.5 to 2.6 ppm nA^{-1}, 3.1 to 3.3 ppm nA^{-1}, and 6.8 to 6.9 ppm nA^{-1}, with a day-to-day variation of <0.1 ppm nA^{-1}. Tuning of the ion source was responsible for the observed differences in H_3^+ factor over the entire sample measuring period. Prior to measuring samples, a *n*-alkane mixture (Mix B, supplied by A. Schimmelmann, Indiana University), which covers a δ^2H range from approximately −50‰ to −250‰, was measured. Sample analyses were only conducted when the average difference and standard deviation between online and offline values was less than 5‰. Squalane and a C_{30} *n*-alkane were coinjected with each sample run for further control on the stability of the system and ranged from −169 ± 3‰ and −78 ± 8‰, respectively, fitting well with their offline established values of −170 ± 4‰ (squalane) and −79 ± 5‰ (C_{30}). High standard deviation for the C_{30} *n*-alkane is attributed to coeluting compounds in the sample fractions. Samples were run in duplicate, and error bars represent the standard errors of duplicate isotope ratio analyses. The RTX-200 60 m column allows for baseline separation of alkenones with different degrees of unsaturation and different chain length. The tri-unsaturated isomers were not baseline separated on the IRMS, but they were well resolved on the GC-FID. Hydrogen isotope ratios presented here are the result of manual peak integrations of all the alkenones for a given chain length (e.g., $\delta^2H_{C37} = C_{37:4}$, $C_{37:3}$, $C_{37:3}$*, and $C_{37:2}$).

2.4. XRF Core Scanning

The inorganic geochemical composition of Core 64PE410-S7 was obtained with an Avaatech X-ray fluorescence (XRF) core scanner at the Royal Netherlands Institute for Sea Research. This XRF core scanner contains a 100 W rhodium X-ray tube and a Rayspec cubed SiriusSD silicon drift detector. Prior to the XRF-core-scan measurements, the sediment surfaces of the core sections were flattened and covered with a 4 μm thin Ultralene foil. For calcium (Ca) and titanium (Ti), the used settings were 10 kV, 0.4 mA, and 10 s, without a primary beam filter. For bromine (Br), the used settings were 30 kV, 0.15 mA, and 10 s, with a thin palladium primary beam filter. The core sections were measured continuously with a 1 cm resolution, excluding some gaps that were caused by gas expansion during core retrieval. The irradiated surface area of the X-Ray beam was set at 1 cm ("down core") by 1.2 cm ("cross core") using the slits of the scanner. All spectral data were processed using the bAxil spectrum analysis software to calculate the element intensities (in counts). The standard tablet SARM-4 was measured before and after each core section, showing that precision was high (relative standard deviation <10%) for all elements targeted here.

2.5. Chronological Framework

The age model for Core 64PE410-S7 is based on a combination of ^{14}C dating and correlation of Ca/Ti and Br records to previously dated, similar records close by (318310: 54°50.34′N; 13°32.03′E, and 318340: 54°55.77′N; 13°41.44′E) (Warden et al., 2016; Figure S1). Bromine is considered to be a good indicator of marine organic carbon content (Ziegler et al., 2008), which can thus be linked to the total organic carbon content obtained through loss on ignition in close-by Core 318310 (Warden et al., 2016). Five important transitions are present within sediments obtained from the Arkona basin (see Warden et al., 2016), which are clearly distinguishable in the carbonate (Ca/Ti) and organic matter (Br and loss on ignition) contents of the

sediment cores (numbered 1 to 5 in Figure S1): first, the transition between the Yoldia Sea and the Ancylus Lake phase at ~10.6 ka; second, the Ancylus Lake regression pinpointed by a peak in organic matter at ~10.2 ka; third, the start of the Ancylus Lake/Littorina Sea transitional phase defined by the increase in organic matter contents at ~7.7 ka; fourth, the transgression maximum indicated by the carbonate maximum at ~7.2 ka; and fifth, the occurrence of a peak in organic matter during the Medieval Climate Anomaly at ~0.9 ka. The first is not present in the core studied here; however, the dip in Ca/Ti content at ~10.5 ka in Core 318340 (Warden et al., 2016) can be linked to that in Core 64PE410-S7 (marked orange in Figure S1). Additionally, we obtained three ^{14}C dates on mollusk shells to improve age control for the interval younger than 7 ka (Figure S1). Shells were radiocarbon dated by Beta Analytic, corrected for the local reservoir effects (reservoir age = 376 years; Lougheed et al., 2013), and calibrated using CALIB (Stuiver et al., 2018). The final age model for all depths was created using the Bacon software package in R (Blaauw & Christen, 2011). In Bacon, the error estimates for ^{14}C ages were also applied to the XRF tie points (as these are based on correlation to the nearby ^{14}C dated cores), and Student's *t* test values were set to 33 and 34 to allow for more narrow error estimates as suggested in the Bacon manual. The resulting age model suggested that sedimentation rates varied between 55 and 250 cm/Kyr over the studied interval. The large variation in sedimentation rates for Core 64PE410-S7 and the nearby cores from Warden et al. (2016) is likely related to the shallow water depth in the Arkona Basin (~45 m). The direction of sediment delivery must have varied over time, with a more northeastward source of sedimentation prior to 7.5 Kyr and a shift to a westward source around 7.5 Kyr. An increase in sedimentation rates around 7.5 Kyr is likely instigated by the marine transgression brought from the North Sea and thus an extra indication of the start of the Littorina Sea phase.

3. Results and Discussion

3.1. Alkenone Distributions

Sediments from the Arkona Basin covering the last 10.6 Kyr were analyzed for long-chain alkenones. Nineteen different alkenones were detected, with chain lengths ranging from 35 to 40 carbon atoms (Table S1). Tri-unsaturated isomers of $C_{37:3}$ methyl and $C_{38:3}$ ethyl alkenones were detected in addition to the conventional $C_{37:3}$ methyl and $C_{38:3}$ ethyl alkenones in some samples. These tri-unsaturated isomers have previously only been reported for lacustrine sediments (Longo et al., 2013, 2016; Dillon et al., 2016; Plancq, Cavazzin, et al., 2018; Plancq, McColl, et al., 2018) and surface sediments in the Baltic Sea basin (Kaiser et al., 2019). Changes in alkenone distribution patterns align with Baltic Sea phase boundaries (Figure 2). Alkenone distributions for the Yoldia Sea phase are typical for Marine Group III, that is, lacking tri-unsaturated isomers as well as C_{39} and C_{40} alkenones (cf. Longo et al., 2013). The first emergence of tri-unsaturated isomers and C_{39} ethyl and methyl alkenones occurs at the Yoldia Sea to Ancylus Lake boundary (Figure 2), signifying the first occurrence of Group I species in this record. The Ancylus Lake distribution is characterized by the presence of tri-unsaturated isomers and C_{39} ethyl and methyl and C_{40} ethyl alkenones (Figure 2). This pattern points to a mixing of Groups I and II haptophytes throughout the Ancylus Lake phase, and distributions are stable across the entire phase. Two samples in the early Ancylus Lake phase show a more marine distribution pattern although still containing the tri-unsaturated isomers indicative of freshwater species. During the Yoldia Sea phase, the southern Baltic experienced short transgressions related to higher sea levels and less continental uplift (Björck, 1995). It appears that the increase in sea level rise overshadowing isostatic rebound also may have continued into the early Ancylus Lake phase, causing some input of saline waters at the onset of this phase.

To constrain the species mixing of Groups I and II haptophytes, the percentage of Groups I and II producers was determined using equation (3), which is based on alkenone distributions in Northern Hemisphere lacustrine sediments and suspended particulate matter (Longo et al., 2018). Group I is indeed dominant throughout the Ancylus Lake phase (57% to 75%), with Group II only contributing substantially at the beginning and the end of the phase (60% to 75%). This is supported by the RIK_{38E} index (equation (2) and Table 1), another indicator of Groups II and I haptophytes (Longo et al., 2016), as it remains below a value of 0.75 which is characteristic for Group I haptophytes.

The transition between the Ancylus Lake and the brackish Littorina Sea phase lasts for ~0.5 Kyr and is characterized by a Group III signature, with only conventional C_{37} methyl and C_{38} ethyl alkenones (Figure 2). However, in the latter half of the transition, the $C_{35:2}$ and $C_{36:2}$ alkenones appear for the first time

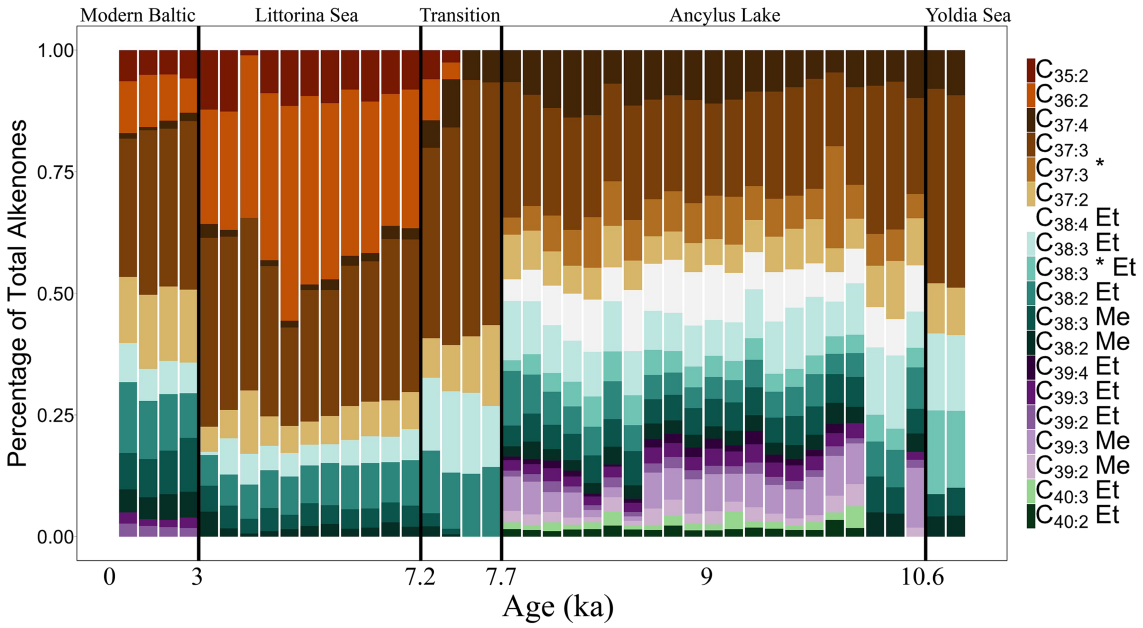

Figure 2. Percent distributions of individual long-chain alkenones present in each sample. The star in the legend indicates the novel tri-unsaturated isomers indicative of Group I alkenone-producers. Alkenones show distinct distributions for each of the Baltic Sea phases.

(Figure 2). The Littorina Sea phase is distinguished from other phases by the presence of the alkenones of shorter chain-length as well as the absence of tri-unsaturated isomers and C_{39} and C_{40} alkenones. The presence of the shorter chain alkenones is an indicator for the presence of Group II haptophytes (Zheng, Dillon, et al., 2016; Zheng, Huang, et al., 2016). The final shift in alkenone distribution corresponds to the change from the Littorina Sea into the Modern Baltic phase and represents a mixed Groups II and III signal indicated by the presence of the $C_{35:2}$, $C_{36:2}$, and C_{39} ethyl alkenones (Figure 2).

Table 1
Alkenone Indices for the Ancylus Lake Phase

Depth (cm)	Age (ka)	RIK_{37}	RIK_{38E}	% Group I	% Group II	% $C_{37:4}$ Salinity (Kaiser et al., 2017)	R3b Salinity (Kaiser et al., 2019)	$U^{K'}_{37}$ Temp. (Müller et al., 1998)	R3b Temp. (Longo et al., 2018)
950	7.76	0.89	0.84	0.25	0.75	6.5	5.3	6.1	5.9
960	7.80	0.82	0.72	0.41	0.59	5.4	4.3	6.6	4.0
964	7.81	0.75	0.72	0.57	0.43	8.9	3.2	6.0	7.4
970	7.84	0.76	0.63	0.55	0.45	4.1	3.4	4.7	5.4
980	7.88	0.67	0.60	0.75	0.25	4.4	2.0	5.8	6.5
990	7.99	0.69	0.63	0.71	0.29	6.2	2.3	7.7	5.7
1,000	8.17	0.74	0.60	0.59	0.41	4.9	3.1	4.9	4.8
1,010	8.35	0.73	0.61	0.62	0.38	4.9	2.9	5.2	5.5
1,020	8.54	0.71	0.64	0.67	0.33	5.1	2.6	5.5	7.2
1,030	8.72	0.72	0.66	0.63	0.37	5.0	2.8	5.3	7.4
1,040	8.90	0.68	0.63	0.72	0.28	4.6	2.2	5.3	7.8
1,050	9.07	0.67	0.67	0.75	0.25	5.1	2.1	5.5	9.2
1,060	9.26	0.74	0.69	0.60	0.40	5.4	3.0	6.4	6.0
1,070	9.44	0.74	0.75	0.59	0.41	5.7	3.1	6.2	8.2
1,080	9.62	0.77	0.77	0.53	0.47	6.0	3.5	6.9	7.1
1,090	9.79	0.79	0.76	0.49	0.51	6.6	3.8	7.3	6.2
1,110	10.14	0.74	0.74	0.59	0.41	5.7	3.1	5.8	7.2
1,120	10.19	0.82	0.72	0.40	0.60	6.5	4.3	5.3	4.0
1,130	10.23	0.82	0.77	0.40	0.60	6.9	4.4	7.2	5.5

Note. Gray shading indicates when Group II species are dominant, and no shading indicates that Group I species are dominant based on the binary mixing model from Longo et al. (2018).

3.2. Temperature and Salinity Estimates

3.2.1. Temperature

The U^{K}_{37} and $U^{K'}_{37}$ indices are well-established sea surface temperature proxies (Brassell et al., 1986; Müller et al., 1998; Prahl & Wakeham, 1987; Rosell-Melé et al., 1995). The latter index excludes the tetra-unsaturated C_{37} alkenone in the equation in response to low concentrations of $C_{37:4}$ in marine sediments. Application of the temperature calibration for the U^{K}_{37} using Atlantic surface sediments (Rosell-Melé et al., 1995) gives negative temperature estimates for this record, while the culture calibration from Prahl and Wakeham (1987) gives a temperature range between 0.3 and 2.3 °C, much lower than present-day spring mean SST of 8 °C (Locarnini et al., 2013). These results are not surprising because the calibrations are based on Group III alkenone distributions characterized by low abundance of the $C_{37:4}$. Groups I and II are known to produce higher concentrations of $C_{37:4}$ (Chivall et al., 2014b; Schulz et al., 2000) which would lead to different calibrations. When excluding the tetra-unsaturated C_{37} alkenones from the equation ($U^{K'}_{37}$ index) and using the global temperature calibration for the $U^{K'}_{37}$ index (Müller et al., 1998), temperature estimates range from 2.2 to 8.5 °C across the record (Figure 3a and Table 1). Haptophytes in the present-day Baltic Sea are known to bloom during the months of April to June (Blanz et al., 2005; Hällfors, 2004), so it is reasonable to expect that alkenones should be reflecting spring temperature values. Modern spring mean temperature is 8 °C (Locarnini et al., 2013), and the most recent sample suggests a temperature of 8.5 °C using the global $U^{K'}_{37}$ calibration, which is in good agreement. Therefore, the $U^{K'}_{37}$ index seems to be the more reliable of the two indices to reconstruct temperatures for this record.

Nevertheless, the presence of different Groups I and II alkenone producers is known to complicate the use of these well-established U^{K}_{37} and $U^{K'}_{37}$ indices in lacustrine and brackish environments (Zheng, Huang, et al., 2016). New indices have been proposed based on Groups I and II distributions that include novel tri-unsaturated isomers in the temperature ratios (Longo et al., 2016, 2018). Since Group I haptophytes are the most abundant in the Ancylus Lake phase (10.6 to 7.7 Kyr), the R3b index seems more applicable for temperature reconstructions during this time period. Using the R3b temperature calibration from Longo et al. (2018), temperature estimates range from 4.0 to 13.5 °C throughout the Ancylus Lake phase, capturing more variation than estimates using the Müller et al. (1998) global calibration for the $U^{K'}_{37}$ index, which range from 4.7 to 7.7 °C (Figure 3a and Table 1).

3.2.2. Salinity

Salinities were reconstructed using $\%C_{37:4}$ for the entire record and the RIK_{37} equation for the Ancylus Lake phase since it was the only phase to contain C_{37} tri-unsaturated isomers (equations (6) and (7), respectively; Kaiser et al., 2017, 2019). Values ranged from 4.1 to 8.7 g kg^{-1} ($\%C_{37:4}$) and 2.0 to 5.2 g kg^{-1} (RIK_{37}), with the $\%C_{37:4}$ yielding slightly higher values (Table 1). The reconstructed salinities based on $\%C_{37:4}$ started to rise at the end of the Ancylus Lake phase leading into the Littorina Sea phase, and both $\%C_{37:4}$ and RIK_{37} calibrations showed an increase in salinities around 7.7 ka during the marine transgression (Figure 3b). In general, $\%C_{37:4}$ suggests a salinity value closest to the modern-day spring mean of 8.1 g kg^{-1} (Zweng et al., 2013) and hence may be the most appropriate for reconstructing salinity of latter part of this record. However, due to the presence of tri-unsaturated isomers during the Ancylus Lake phase, the RIK_{37} salinity calibration might provide better estimates during this phase, since it includes the tri-unsaturated isomers. Indeed, using the RIK_{37} calibration yielded an average salinity of 3 ± 0.4 g kg^{-1}, which seems more logical than an average of 6 ± 0.5 g kg^{-1} (obtained from the $\%C_{37:4}$ calibration) for this relatively fresh phase in the Baltic Sea history (Jensen et al., 1999). The Ancylus Lake phase in the Arkona Basin was dominated by lacustrine macrofossils, diatoms, and sedimentary deposits (Jensen et al., 1999), reinforcing a low salinity to even freshwater environment. Furthermore, the $\%C_{37:4}$ shows more fluctuations in salinity, whereas the RIK_{37} suggests a more steady decrease in salinity, in line with a gradual shift from a brackish into a lacustrine, freshwater environment during the Early Ancylus Lake phase. In general, when tri-unsaturated isomers are present, indices accounting for these isomers seem more appropriate for reconstructing temperature and salinity. The above observations confirm the necessity of obtaining optimal separation of individual alkenones to enable detection of these informative isomers.

Salinities reconstructed using the $\%C_{37:4}$ equation from Kaiser et al. (2017) align well with modern-day salinity values for the Arkona Basin. That being said, reconstructed values are relatively stable at around 8 g kg^{-1} across the Littorina Sea phase, a period of higher salinity than either the Ancylus Lake or Modern

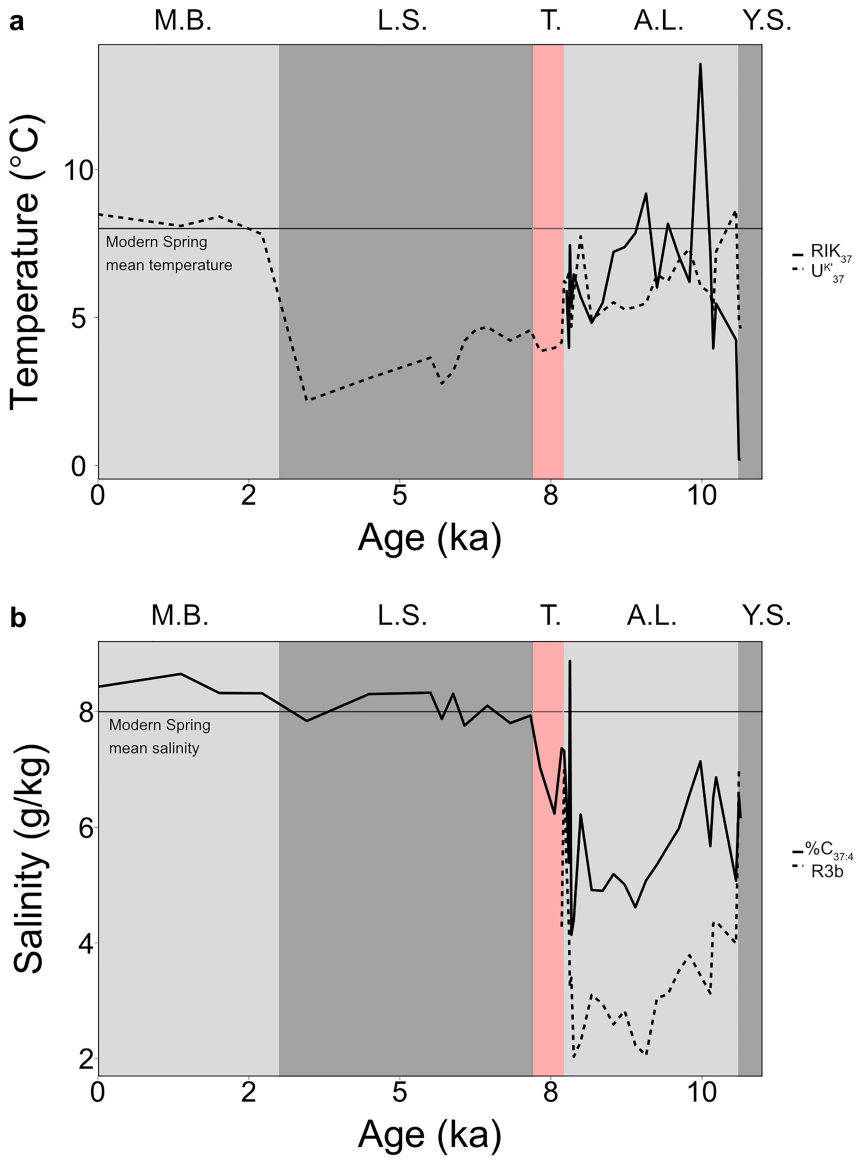

Figure 3. (a) Comparison of reconstructed temperatures based on the well-established $U^{K'}_{37}$ index and the newly proposed R3b index (Longo et al., 2018). The R3b index includes the tri-unsaturated C_{37} and C_{38} isomers and was therefore only applied to samples containing said isomers. (b) Reconstructed salinities using the Baltic Sea $\%C_{37:4}$ calibration (Kaiser et al., 2017) and the RIK_{37} calibration (Kaiser et al., 2019), both from Baltic Sea surface sediments. Similar to the R3b temperature index, the RIK_{37} index includes the tri-unsaturated C_{37} isomer, thus was only applied to samples containing the tri-unsaturated C_{37} isomer. Present-day spring mean temperature (8 °C) and salinity (8.1 g kg^{-1}) from the World Ocean Atlas 2013 (Locarnini et al., 2013; Zweng et al., 2013) are denoted by the dotted line, and abbreviations for corresponding Baltic Sea phases are at the top.

Baltic phases as the result of increased North Sea inflow (Emeis et al., 2003). This strong marine influence is not obvious in the $\%C_{37:4}$ based record. Haptophyte species produce different relative amounts of the $C_{37:4}$ alkenone, and these differences are even noted between species from the same group—for example, *I. galbana* was shown to have a relative abundance of $C_{37:4}$ around 5% to 10% and *R. lamellosa* around 35% to 40% (Chivall et al., 2014b). The changing haptophyte community composition affects the relative abundance of these alkenones potentially leading to such stable salinity estimates across the higher salinity Littorina Sea phase into the fresher Modern Baltic phase.

3.3. Hydrogen Isotope Ratios

Hydrogen isotope ratios of integrated C_{37} and C_{38} alkenones, and for the $C_{36:2}$ alkenones when present, were measured (Table 2, Figure 4). Isotope ratios for all C_{37} and C_{38} were integrated. δ^2H values of C_{37} and C_{38} showed two major shifts: a substantial enrichment of ~50‰ starting at approximately 10 ka (mid-Ancylus Lake phase) and a depletion of ~25‰ at around 3 ka (Littorina Sea to Modern Baltic phase boundary). The $C_{36:2}$ first occurred at the start of the Littorina Sea phase, and δ^2H values were similar to those of the C_{37} alkenones. The δ^2H values of the $C_{36:2}$ became enriched across the transition from the Littorina Sea into the Modern Baltic phase by around 15‰, deviating from the C_{37} and C_{38} alkenones which became increasingly depleted by as much as 40‰ in the most modern sample at 1.37 ka (Figure 4). It has been hypothesized that the $C_{36:2}$ ethyl alkenone is synthesized from the $C_{38:2}$ ethyl alkenones by β-oxidation (Zheng, Dillon, et al., 2016). During the Littorina Sea phase, there was relative isotopic enrichment of the C_{38} compared to the C_{36}, but this reversed in the Modern Baltic phase. It might be the case that when $C_{36:2}$ is synthesized from $C_{38:2}$, the loss of four hydrogens via β-oxidation causes the C_{36} to become relatively ^2H depleted. In the more modern phase, there might be a greater amount of C_{38} produced by a different species (Group III), causing relative depletion of the C_{38} pool which overwrites this degradation effect.

The two isotopic shifts observed for the C_{37} and C_{38} alkenones (at approximately 3 and 10 ka) reveal two separate effects that do not coincide with large shifts in reconstructed salinity values. Reconstructed salinities were stable from the Littorina Sea into the Modern Baltic phase at the Arkona Basin. The shift toward more negative values at 3 ka aligns with the phase boundary between the Littorina Sea and the Modern Baltic phase and coincides with a shift in the alkenone producing population from Group II dominance to a mixed Groups II and III signal noted by changes in distributions (Figure 2). As explained above, the C_{37} and C_{38} alkenones differ from the $C_{36:2}$ by up to 40‰ in the most modern sample. Our isotope data from the Modern Baltic phase cannot confirm the synthesis of $C_{36:2}$ from $C_{38:2}$ via β-oxidation because values do not align with ratios proposed by Zheng, Dillon, et al. (2016; Figure S2) and instead suggest mixing of different haptophyte groups contributing alkenones to the sedimentary alkenone pool. Each group has a characteristic isotopic range measured from culture experiments (Schouten et al., 2006; Chivall et al., 2014a, 2014b; M'Boule et al., 2014; Sachs et al., 2016; Weiss et al., 2017). Group II spans a range of −189‰ to −97‰ over a salinity gradient from 10 to 35, and Group III values span from −263‰ to −173‰ over a salinity gradient from 24 to 42. As salinity becomes lower, more depleted isotope ratios for C_{37} and C_{38} alkenones are expected due to a lowering of the δ^2H of the water as well as increased isotopic fractionation (Schouten et al., 2006; Chivall et al., 2014a, 2014b; M'Boule et al., 2014; Sachs et al., 2016; Weiss et al., 2017). Compiled Group III culture data (M'Boule et al., 2014; Sachs et al., 2016; Schouten et al., 2006; Weiss et al., 2017) together with the sea water δ^2H values suggest that salinities of 7 to 8 g kg^{-1} result in isotope ratios of around −218‰, close to measured values for this interval. Group II species, on the other hand, tend to have more enriched isotope ratios at these salinities (around −186‰; based on results from Chivall et al., 2014a, 2014b, and M'Boule et al., 2014). The presence of the $C_{36:2}$ implies Group II contribution to the sedimentary alkenone pool. While the $C_{36:2}$ isotope ratios have not been reported from culture experiments, the similarity between $C_{36:2}$ with both the C_{37} and C_{38} during the Littorina Sea phase suggests that when produced by Group II species, the three do not differ by more than ~15‰. Collectively, these observations imply that the isotope shift at 3 ka is caused by a change in species composition.

The large isotope enrichment of ~50‰ starting at 10 ka occurs in the middle of the Ancylus lake phase and does not coincide with a change in alkenone distributions, and hence, the alkenone distribution-based salinity estimates show no large fluctuations (Figures 2 and 3). Group II culture regressions suggest δ^2H values should be around −210‰ for a salinity of zero (Chivall et al., 2014a, 2014b; M'Boule et al., 2014). This value is more enriched than values measured for the early Ancylus Lake phase; thus, an alternative mechanism must be invoked to explain the depleted values measured for this freshwater phase in Baltic Sea history. Source water isotope ratios also exhibit a strong control on δ^2H values (Englebrecht & Sachs, 2005; Paul, 2002). During this time period, the Scandinavian Ice Sheet was rapidly decreasing in size, as a result of an increase in high latitude summer insolation and changes in ablation rates (Cuzzone et al., 2016). The melting Scandinavian Ice Sheet acted as an additional water source for the Baltic Sea. The Scandinavian Ice Sheet formed during the last glacial and was significantly depleted in hydrogen isotope ratios with a δ^2H value of around −310‰ suggested by modeling data (de Boer et al.,

Table 2
Hydrogen Isotope Ratios of $C_{36:2}$ and the integrated C_{37} and C_{38} Alkenones

Depth (cm)	Age (ka)	$\delta^2H_{C36:2}$ (‰ vs. VSMOW)	Standard error	δ^2H_{C37} (‰ vs. VSMOW)	Standard error	δ^2H_{C38} (‰ vs. VSMOW)	Standard error
120	1.37	−173	2	−212	4	−208	1
320	2.71	−182	3	−209	1	−191	7
420	3.46	−188	2	−184	2	−173	1
600	5.31	−176	0	−181	3	−159	10
620	5.50	−179	1	−190	1	−182	4
640	5.69	−176	1	−180	5	−160	19
660	5.90	−178	0	−187	2	−167	12
700	6.26	−184	2	−193	3	−183	7
760	6.83	−191	3	−190	6	−172	3
800	7.16	−186	3	−191	3	−180	4
840	7.32	−172	1	−189	8	−189	1
900	7.56	—	—	−192	1	−200	3
930	7.68	—	—	−196	2	−193	2
940	7.72	—	—	−197	3	−189	2
950	7.76	—	—	−199	0	−193	4
960	7.80	—	—	−188	2	−195	1
964	7.81	—	—	−191	4	−191	2
970	7.84	—	—	−190	1	−196	3
980	7.88	—	—	−191	1	−193	14
1,000	8.17	—	—	−186	1	−178	4
1,010	8.35	—	—	−184	0	−177	0
1,020	8.54	—	—	−183	1	−177	3
1,030	8.72	—	—	−194	3	−182	0
1,040	8.90	—	—	−187	1	−179	5
1,050	9.07	—	—	−197	2	−202	2
1,060	9.26	—	—	−193	1	−205	1
1,070	9.44	—	—	−206	0	−201	0
1,080	9.62	—	—	−233	3	−238	2
1,090	9.79	—	—	−242	2	−252	3
1,100	9.97	—	—	−231	4	−251	4
1,110	10.14	—	—	−241	0	−233	7
1,120	10.19	—	—	−239	2	−233	1
1,200	10.56	—	—	−230	1	−224	2
1,210	10.61	—	—	−228	3	−214	4
1,216	10.64	—	—	−233	5	−211	1

2014). Holocene Baltic Sea precipitation has a value of −68.1 ± 0.7‰ (Fröhlich et al., 1988), significantly more enriched compared to the melting Scandinavian Ice Sheet in the Early Holocene. The difference between these two sources is large enough that a relatively modest, yet substantial, contribution of ice melt-derived source water would be reflected in δ^2H_{C37} values, resulting in significant isotopic depletion (Figure 4). The steep decline in δ^2H_{C37} values seems to indicate a rather rapid phase of melting of the Scandinavian Ice Sheet, which disappeared completely at about 9.5 ka (Figure 5). The largest part of the Scandinavian ice sheet melted before this time. This major melting phase seems to be recorded in the hydrogen isotopic composition of only the C_{38} alkenones. Prior to the 50‰ isotope shift, the water in the Arkona Basin was derived from a combination of rain water and melt water from the ice sheet, which explains the relatively depleted values during this period. Only at the end of the melting phase does the relative contribution of melt water drop significantly, reflected as an enrichment in the hydrogen isotopic composition of the Arkona Basin water and in turn recorded by alkenone hydrogen isotopes.

To constrain this, the δ^2H values of source water can be reconstructed using calibration data from haptophyte cultures and a simple end-member mixing model with meltwater and precipitation together contributing to the Baltic Sea water. The offset between δ^2H values of water and the δ^2H values of alkenones is not constant and is affected by biological fractionation (fractionation factor α) occurring during alkenone synthesis (Schouten et al., 2006; Chivall et al., 2014a, 2014b; M'Boule et al., 2014; Sachs et al., 2016; Weiss et al.,

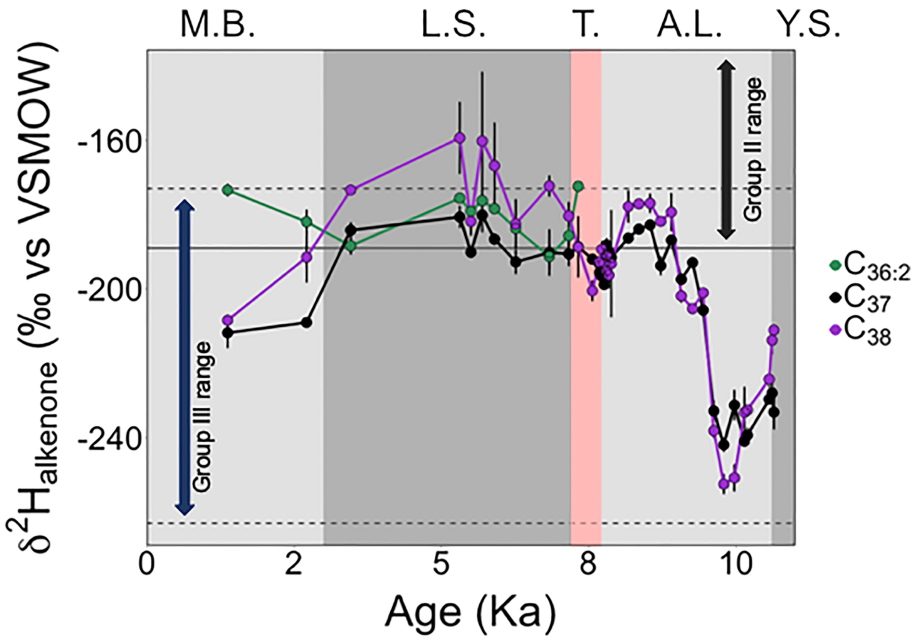

Figure 4. Hydrogen isotopes ratios of $C_{36:2}$ and integrated C_{37} and C_{38} alkenones over the last 10.6 Kyr in the Arkona Basin. Two major isotope shifts occur: The C_{37} and C_{38} alkenones become significantly enriched in the middle of the Ancylus Lake phase, and the $C_{36:2}$ deviates from the C_{37} and C_{38} at the Littorina Sea to Modern Baltic phase shift. Error bars represent reproducibility of duplicate hydrogen isotope analyses.

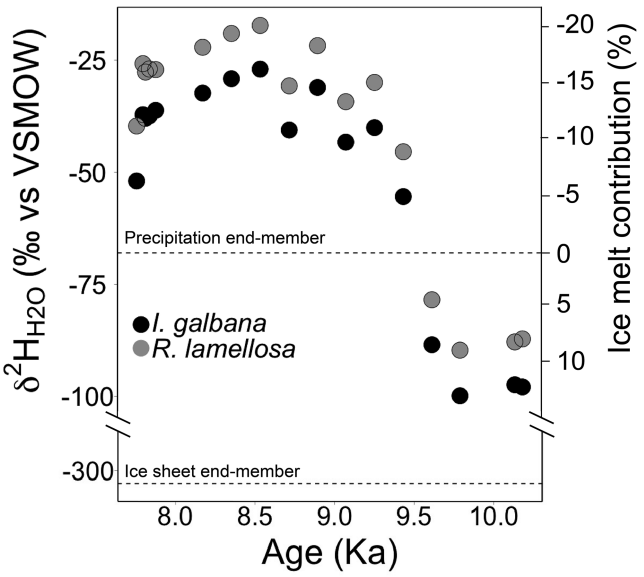

Figure 5. Reconstructed hydrogen isotope ratios of water plotted alongside the corresponding ice melt contribution during the Ancylus Lake phase. Ice melt contribution was calculated using a simple two end-member mixing model, with modeled Scandinavian Ice Sheet values and modern precipitation ratios as the two end-members. We accounted for fractionation values using results from cultures of two different Group II species *Isochrysis galbana* and *Ruttnera lamellosa*. Percent contribution of ice becomes negative, suggesting that the Scandinavian Ice Sheet no longer contributed water to the Baltic Sea after 9.5 ka and was replaced by a much lighter source.

2017). The fractionation factor α from two Group II species *I. galbana* and *R. lamellosa* at a salinity of around 3 g kg^{-1} (value obtained from the alkenone estimates; Figure 3) is 0.841 and 0.832, respectively (Chivall et al., 2014a, 2014b; M'Boule et al., 2014). It should be noted that the presence of Group I alkenone distributions indicates freshwater conditions, thus salinities between 2 and 5 may not be accurate, but these estimates will be used for roughly determining the δ^2H values of source water. Assuming this fractionation value and using the measured δ^2H values of alkenones across the ~50‰ shift, we calculated that the δ^2H values of the water should change from −99‰ to −40‰ using *I. galbana* α values and −89‰ to −30‰ using *R. lamellosa* α values. Following this, we could estimate the percent contribution of both ice melt-derived source water and precipitation using −310‰ (ice) and −68‰ (precipitation) as end-members. As expected, it showed that there was a decrease in the percent contribution from ice melt-derived source water starting at approximately 10 ka (Figure 5). However, reconstructed contributions exceed 100% (precipitation) or go into negative values (ice) at some points, suggesting that a freshwater source with a heavier δ^2H value than that of modern precipitation must have been present. Indeed, a rise in water level during this time period coincides with the creation of the Dana River, suggesting another freshwater source between 9.5 and 9.0 ka (Björck, 1995). Thus, a more ^2H-enriched freshwater end-member might not be unrealistic. Still, these values cannot fully explain the observed range in δ^2H_{H2O} values. This would either require a heavier precipitation source, which is not likely in view of the reconstructed temperatures, or admixing of some sea water. The sea water either somehow entered the basin (although it was closed off from the North Sea during this time), or some sea water

remained from an earlier, more saline phase in the basin (i.e., Yoldia Sea). Regardless of the δ^2H values of both (or three when including sea water) end-members, it can be estimated that the freshwater input directly from the melting Scandinavian Ice Sheet ceased to contribute to the freshwater budget around 9.5 ka. The R3b index indicated a spike in temperature coincident with the shift in source water, suggesting that temperatures might have locally increased in response to the ice sheet being fully melted, which directly affected the local albedo.

4. Conclusions

A large number of alkenone isomers were detected in Holocene age sediments from the Arkona Basin using improved gas chromatography separation, allowing for better determination of the haptophyte population in the Holocene Baltic Sea. Tri-unsaturated isomers, indicative of Group I alkenone producers, were prominent during the Ancylus Lake freshwater phase from 10.6 to 7.7 ka. For this reason, temperature and salinity calibrations based on indices including tri-unsaturated isomers provide more reliable estimates during this time period, circumventing issues associated with traditional alkenone-based temperature indices (i.e., anomalously high or low temperatures). Changes in distribution show mixing between Groups III and II in the Yoldia Sea, Littorina Sea, and Modern Baltic phases.

Hydrogen isotope ratios of long-chain alkenones inform about changes in salinity and species composition but also provided insight into shifts in the dominant freshwater sources at the Arkona Basin. Results presented here show that analysis of well-separated alkenone distributions, in conjunction with hydrogen isotope ratios, provide a more in-depth understanding of species, salinity, and hydrological changes in paleoenvironmental settings, especially in marginal marine environments.

Acknowledgments
The captain and crew of the RV Pelagia are thanked for their help with obtaining the piston core used in the present investigation. We thank Editor Adina Paytan, Dr. Jaime Toney, and an anonymous reviewer for their comments which improved the manuscript. This study received funding from the Netherlands Earth System Science Center (NESSC) though a Gravitation grant (024.002.001) from the Dutch Ministry for Education, Culture and Science. All acquired data are stored in the Royal Netherlands Institute for Sea Research (NIOZ) database which can be accessed at data-verse.nioz.nl (DOI: 10.25852/nioz/7b.b.q).

References

Andrén, E., Andrén, T., & Sohlenius, G. (2000). The Holocene history of the southwestern Baltic Sea as reflected in a sediment core from the Bornholm Basin. *Boreas*, *29*, 233–250. https://doi.org/10.1111/j.1502-3885.2000.tb00981.x

Araie, H., Nakamura, H., Toney, J. L., Haig, H. A., Plancq, J., Takashi, S., et al. (2018). Novel alkenone-producing strains of the genus Isochrysis (Haptophyta) isolated from Canadian saline lakes show temperature sensitivity of alkenones and alkenoates. *Organic Geochemistry*, *121*, 80–103. https://doi.org/10.1016/j.orggeochem.2018.04.008

Björck, S. (1995). A review of the history of the Baltic Sea, 13.0-8.0 ka BP. *Quaternary International*, *27*, 19–40. https://doi.org/10.1016/1040-6182(94)00057-C

Blaauw, M., & Christen, J. A. (2011). Flexible paleoclimate age-depth models using an autoregressive gamma process. *Bayesian analysis*, *6*(3), 457–474. https://doi.org/10.1214/ba/1339616472

Blanz, T., Emeis, K. C., & Siegel, H. (2005). Controls on alkenone unsaturation ratios along the salinity gradient between the open ocean and the Baltic Sea. *Geochimica et Cosmochimica Acta*, *69*, 3589–3600. https://doi.org/10.1016/j.gca.2005.02.026

de Boer, B., Stocchi, P., & van de Wal, R. S. W. (2014). A fully coupled 3-D ice-sheet-sea-level model: Algorithm and applications. *Geoscientific Model Development*, *7*, 2141–2156. https://doi.org/10.5194/gmd-7-2141-2014

Brassell, S. C., Eglinton, G., Marlowe, I. T., Pflaumann, U., & Sarnthein, M. (1986). Molecular stratigraphy: A new tool for climatic assessment. *Nature*, *320*, 129–133. https://doi.org/10.1038/320129a0

Chivall, D., M'Boule, D., Sinke-Schoen, D., Sinninghe Damsté, J. S., Schouten, S., & van der Meer, M. T. J. (2014a). The effects of growth phase and salinity on the hydrogen isotopic composition of alkenones produced by coastal haptophyte algae. *Geochimica et Cosmochimica Acta*, *140*, 381–390. https://doi.org/10.1016/j.gca.2014.05.043

Chivall, D., M'Boule, D., Sinke-Schoen, D., Sinninghe Damsté, J. S., Schouten, S., & van der Meer, M. T. J. (2014b). Impact of salinity and growth phase on alkenone distributions in coastal haptophytes. *Organic Geochemisty*, *67*, 31–34. https://doi.org/10.1016/j.orggeochem.2013.12.002

Cuzzone, J. K., Clark, P. U., Carlson, A. E., Ullman, D. J., Rinterknecht, V. R., Milne, G. A., et al. (2016). Final deglaciation of the Scandinavian Ice Sheet and implications for the Holocene global sea-level budget. *Earth and Planetary Science Letters*, *448*, 36–41. https://doi.org/10.1016/j.epsl.2016.05.019

Dillon, J. T., Longo, W. M., Zhang, Y., Torozo, R., & Huang, Y. (2016). Identification of double-bond positions in isomeric alkenones from a lacustrine haptophyte. *Rapid Communications in Mass Spectrometry*, *30*(1), 112–118. https://doi.org/10.1002/rcm.7414

Emeis, K.-C., Struck, U., Blanz, T., Kohly, A., & Voß, M. (2003). Salinity changes in the central Baltic Sea (NW Europe) over the last 10,000 years. *The Holocene*, *13*, 411–421. https://doi.org/10.1191/0959683603hl634rp

Englebrecht, A. C., & Sachs, J. P. (2005). Determination of sediment provenance at drift sites using hydrogen isotopes and unsaturation ratios in alkenones. *Geochimica et Cosmochimica Acta*, *69*, 4253–4265. https://doi.org/10.1016/j.gca.2005.04.011

Fröhlich, K., Grabczak, J., & Rozankski, K. (1988). Deuterium and oxygen-18 in the Baltic Sea. *Chemical Geology*, *72*, 77–83. https://doi.org/10.1016/0168-9622(88)90038-3

Fujine, K., Yamamoto, M., Tada, R., & Kido, Y. (2006). A salinity-related occurrence of a novel alkenone and alkenoate in Late Pleistocene sediments from the Japan Sea. *Organic Geochemistry*, *37*(9), 1074–1084. https://doi.org/10.1016/j.orggeochem.2006.05.004

Hällfors, G. (2004). Checklist of Baltic Sea phytoplankton species (including some heterotrophic protistan groups). Helsinki Commission, Baltic Marine Environment Protection Commission.

Jensen, J. B., Bennike, O., Witkowski, A., Lemke, W., & Kuijpers, A. (1999). Early Holocene history of the southwestern Baltic Sea: The Ancylus Lake stage. *Boreas*, *28*(4), 437–453. https://doi.org/10.1111/j.1502-3885.1999.tb00233.x

Jordan, R. W., & Chamberlain, A. H. L. (1997). Biodiversity among haptophyte algae. *Biodiversity and Conservation*, *6*(1), 131–152. https://doi.org/10.1023/A:1018383817777

Kaiser, J., van der Meer, M. T. J., & Arz, H. W. (2017). Long-chain alkenones in Baltic Sea surface sediments: New insights. *Organic Geochemistry*, *112*, 93–104. https://doi.org/10.1016/j.orggeochem.2017.07.002

Kaiser, J., Wang, K. J., Rott, D., Li, G., Zheng, Y., Amaral-Zettler, L., et al. (2019). Changes in long chain alkenone distributions and Isochrysidales groups along the Baltic Sea salinity gradient. *Organic Geochemistry*, *127*, 92–103. https://doi.org/10.1016/j.orggeochem.2018.11.012

Kasper, S., van der Meer, M. T. J., Castañeda, I. S., Tjallingii, R., Brummer, G. J. A., Sinninghe Damsté, J. S., & Schouten, S. (2015). Testing the alkenone D/H ratio as a paleo indicator of sea surface salinity in a coastal ocean margin (Mozambique Channel). *Organic Geochemistry*, *78*, 62–68. https://doi.org/10.1016/j.orggeochem.2014.10.011

Kasper, S., van der Meer, M. T. J., Mets, A., Zahn, R., Sinninghe Damsté, J. S., & Schouten, S. (2014). Salinity changes in the Agulhas leakage area recorded by stable hydrogen isotopes of C_{37} alkenones during Termination I and II. *Climate of the Past*, *10*, 251–260. https://doi.org/10.5194/cp-10-251-2014

Laguna, R., Romo, J., Read, B. A., & Wahlund, T. M. (2001). Induction of phase variation events in the life cycle of the marine coccolithophorid *Emiliania huxleyi*. *Applied and Environmental Microbiology*, *67*(9), 3824–3831. https://doi.org/10.1128/AEM.67.9.3824.3831.2001

Leduc, G., Sachs, J. P., Kawka, O. E., & Schneider, R. R. (2013). Holocene changes in eastern equatorial Atlantic salinity as estimated by water isotopologues. *Earth and Planetary Science Letters*, *362*, 151–162. https://doi.org/10.1016/j.epsl.2012.12.003

de Leeuw, J. W., van der Meer, F. W., Rijpstra, W. I. C., & Schenck, P. A. (1980). On the occurrence and structural identification of long chain unsaturated ketones and hydrocarbons in sediments. In A. G. Douglas, & J. R. Maxwell (Eds.), *Advances in organic geochemistry 1979*, (pp. 211–217). Oxford: Pergamon Press. https://doi.org/10.1016/0079-1946(79)90105-8

Locarnini, R. A., Mishonov, A. V., Antonov, J. I., Boyer, T. P., Garcia, H. E., Baranova, O. K., Zweng, M. M., Paver, C. R., Reagan, J. R., Johnson, D. R., Hamilton, M., & Seidov, D. (2013). *World Ocean Atlas 2013, Volume 1: Temperature*. S. Levitus & A. Mishonov (Eds.). *Technical Ed.* (pp. 40). Silver Spring, MD: NOAA Atlas NESDIS 73.

Longo, W. M., Dillon, J. T., Tarozo, R., Salacup, J. M., & Huang, Y. (2013). Unprecedented separation of long chain alkenones from gas chromatography with a poly (trifluoropropylmethylsiloxane) stationary phase. *Organic Geochemistry*, *65*, 94–102. https://doi.org/10.1016/j.orggeochem.2013.10.011

Longo, W. M., Huang, Y., Yao, Y., Zhao, J., Giblin, A. E., Wang, X., et al. (2018). Widespread occurrence of distinct alkenones from Group I haptophytes in freshwater lakes: Implications for paleotemperature and paleoenvironmental reconstructions. *Earth and Planetary Science Letters*, *492*, 239–250. https://doi.org/10.1016/j.epsl.2018.04.002

Longo, W. M., Theroux, S., Giblin, A. E., Zheng, Y., Dillon, J. T., & Huang, Y. (2016). Temperature calibration and phylogenetically distinct distributions for freshwater alkenones: Evidence from northern Alaskan lakes. *Geochimica et Cosmochimica Acta*, *180*, 177–196. https://doi.org/10.1016/j.gca.2016.02.019

Lougheed, B. C., Filipsson, H. L., & Snowball, I. (2013). Large spatial variations in coastal ^{14}C reservoir age—A case study from the Baltic Sea. *Climate of the Past*, *9*, 1015–1028. https://doi.org/10.5194/cp-9-1015-2013

M'Boule, D., Chivall, D., Sinke-Schoen, D., Sinninghe Damsté, J. S., Schouten, S., & van der Meer, M. T. J. (2014). Salinity dependent hydrogen isotope fractionation in alkenones produced by coastal and open ocean haptophyte algae. *Geochimica et Cosmochimica Acta*, *130*, 126–135. https://doi.org/10.1016/j.gca.2014.01.029

van der Meer, M. T. J., Baas, M., Rijpstra, W. I. C., Marino, G., Rohling, E. J., Sinninghe Damsté, J. S., & Schouten, S. (2007). Hydrogen isotopic compositions of long-chain alkenones record freshwater flooding of the Eastern Mediterranean at the onset of sapropel deposition. *Earth and Planetary Science Letters*, *262*, 594–600. https://doi.org/10.1016/j.epsl.2007.08.014

van der Meer, M. T. J., Benthein, A., French, K. L., Epping, E., Zondervan, I., Reichart, G. J., et al. (2015). Large effect of irradiance on hydrogen isotope fractionation of alkenones in *Emiliania huxleyi*. *Geochimica et Cosmochimica Acta*, *160*, 16–24. https://doi.org/10.1016/j.gca.2015.03.024

van der Meer, M. T. J., Sangiorgi, F., Baas, M., Brinkhuis, H., Sinninghe Damsté, J. S., & Schouten, S. (2008). Molecular isotopic and dinoflagellate evidence for Late Holocene freshening of the Black Sea. *Earth and Planetary Science Letters*, *267*(3-4), 426–434. https://doi.org/10.1016/j.epsl.2007.12.001

Mörner, N.-A. (1995). The Baltic Ice Lake–Yoldia Sea transition. *Quaternary International*, *27*, 95–98. https://doi.org/10.1016/1040-6182(94)00065-D

Moros, M., Lemke, W., Kuijpers, A., Endler, R., Jensen, J. B., Bennike, O., & Gingele, F. (2002). Regressions and transgressions of the Baltic basin reflected by a new high-resolution deglacial and postglacial lithostratigraphy for Arkona Basin sediments (western Baltic Sea). *Boreas*, *31*, 151–162. https://doi.org/10.1080/030094802320129953

Müller, P. J., Kirst, G., Ruhland, G., Von Storch, I., & Rosell-Melé, A. (1998). Calibration of the alkenone paleotemperature index $U^{K'}_{37}$ based on core-tops from the eastern South Atlantic and the global ocean (60° N-60° S). *Geochimica et Cosmochimica Acta*, *62*, 1757–1772. https://doi.org/10.1016/S0016-7037(98)00097-0

Nelson, D. B., & Sachs, J. P. (2014). The influence of salinity on D/H fractionation in alkenones from saline and hypersaline lakes in continental North America. *Organic Geochemistry*, *66*, 38–47. https://doi.org/10.1016/j.orggeochem.2013.10.013

Paasche, E. (2002). A review of the coccolithophorid *Emiliania huxleyi* (Prymnesiophyceae) with particular reference to growth, coccolith formation, and calcification-photosynthesis interactions. *Phycologia*, *40*, 503–529. https://doi.org/10.2216/i0031-8884-40-6-503.1

Pahnke, K., Sachs, J. P., Keigwin, L., Timmermann, A., & Xie, S. P. (2007). Eastern tropical Pacific hydrologic changes during the past 27,000 years from D/H ratios in alkenones. *Paleoceanography*, *22*(4). https://doi.org/10.1029/2007PA001468

Paul, H. (2002). Application of novel stable isotope methods to reconstruct paleoenvironments, Compound specific hydrogen isotopes and pore-water oxygen isotopes. PhD thesis, Swiss Federal Institute of Technology.

Petrick, B. F., McClymont, E. L., Marret, F., & van der Meer, M. T. J. (2015). Changing surface water conditions for the last 500 ka in the Southeast Atlantic: Implications for variable influences of Agulhas leakage and Benguela upwelling. *Paleoceanography*, *30*, 1153–1167. https://doi.org/10.1002/2015PA002787

Plancq, J., Cavazzin, B., Juggins, S., Haig, H. A., Leavitt, P. R., & Toney, J. L. (2018). Assessing environmental controls on the distribution of long-chain alkenones in the Canadian Prairies. *Organic Geochemistry*, *117*, 43–55. https://doi.org/10.1016/j.orggeochem.2017.12.005

Plancq, J., McColl, J. L., Bendle, J. A., Seki, O., Cuoto, J. M., Henderson, A. C. G., et al. (2018). Genomic identification of the long-chain alkenone producer in freshwater Lake Toyoni, Japan: implications for temperature reconstructions. *Organic Geochemistry*, *125*, 189–195. https://doi.org/10.1016/j.orggeochem.2018.09.011

Prahl, F. G., Rontani, J. F., Volkman, J. K., Sparrow, M. A., & Royer, I. M. (2006). Unusual C_{35} and C_{36} alkenones in a paleoceanographic benchmark strain of *Emiliania huxleyi*. *Geochimica et Cosmochimica Acta*, *70*(11), 2856–2867. https://doi.org/10.1016/j.gca.2006.03.009

Prahl, F. G., & Wakeham, S. G. (1987). Calibration of unsaturation patterns in long-chain ketone compositions for palaeotemperature assessment. *Nature*, *330*(6146), 367. https://doi.org/10.1038/330367a0

Rontani, J. F., Marchand, D., & Volkman, J. K. (2001). $NaBH_4$ reduction of alkenones to the corresponding alkenols: A useful tool for their characterisation in natural samples. *Organic Geochemistry*, *32*(11), 1329–1341. https://doi.org/10.1016/S0146-6380(01)00091-2

Rosell-Melé, A., Eglinton, G., Pflaumann, U., & Sarnthein, M. (1995). Atlantic core-top calibration of the U^K_{37} index as a sea-surface palaeotemperature indicator. *Geochimica et Cosmochimica Acta*, *59*(15), 3099–3107. https://doi.org/10.1016/0016-7037(95)00199-A

Sachs, J. P., & Kawka, O. E. (2015). The influence of growth rate on $^2H/^1H$ fractionation in continuous cultures of the coccolithophorid *Emiliania huxleyi* and the diatom *Thalassiosira pseudonana*. *PLoS One*, *10*(11), e0141643. https://doi.org/10.1371/journal.pone.0141643

Sachs, J. P., Maloney, A. P., Gregersen, J., & Paschall, C. (2016). Effect of salinity on $^2H/^1H$ fractionation in lipids from continuous cultures of the coccolithophorid *Emiliania huxleyi*. *Geochimica et Cosmochimica Acta*, *189*, 96–109. https://doi.org/10.1016/j.gca.2016.05.041

Schouten, S., Ossebar, J., Shreiber, K., Kienhuis, M. V. M., Benthien, A., & Bijma, J. (2006). The effect of temperature, salinity and growth rate on the stable hydrogen isotopic composition of long chain alkenones produced by *Emiliania huxleyi* and *Gephyrocapsa oceanica*. *Biogeosciences*, *3*, 113–119. https://doi.org/10.5194/bg-3-113-2006

Schulz, H. M., Schöner, A., & Emeis, K. C. (2000). Long-chain alkenone patterns in the Baltic Sea—An ocean-freshwater transition. *Geochimica et Cosmochimica Acta*, *64*, 469–477. https://doi.org/10.1016/S0016-7037(99)00332-4

Schwab, V. F., & Sachs, J. P. (2011). Hydrogen isotopes in individual alkenones from the Chesapeake Bay estuary. *Geochimica et Cosmochimica Acta*, *75*, 7552–7565. https://doi.org/10.1016/j.gca.2011.09.031

Simon, M. H., Gong, X., Hall, I. R., Ziegler, M., Barker, S., Knorr, G., et al. (2015). Salt exchange in the IndianAtlantic Ocean Gateway since the Last Glacial Maximum: A compensating effect between Agulhas Current changes and salinity variations? *Paleoceanography*, *30*, 1318–1327. https://doi.org/10.1002/2015PA002842

van Soelen, E. E., Lammers, J. M., Eglinton, T. I., Sinninghe Damsté, J. S., & Reichart, G. J. (2014). Unusual C_{35} to C_{38} alkenones in mid-Holocene sediments from a restricted estuary (Charlotte Harbor, Florida). *Organic Geochemistry*, *70*, 20–28. https://doi.org/10.1016/j.orggeochem.2014.01.021

Stuiver, M., Reimer, P. J., & Reimer, R. W. (2018). CALIB 7.1 [WWW program] at http://calib.org, accessed 2018-11-7.

Theroux, S., D'Andrea, W. J., Toney, J., Amaral-Zettler, L., & Huang, Y. (2010). Phylogenetic diversity and evolutionary relatedness of alkenone-producing haptophyte algae in lakes: Implications for continental paleotemperature reconstructions. *Earth and Planetary Science Letters*, *300*(3-4), 311–320. https://doi.org/10.1016/j.epsl.2010.10.009

Tierney, J. E., & Tingley, M. P. (2018). BAYSPLINE: A new calibration for the alkenone paleothermometer. *Paleoceanography*, *33*, 281–301. https://doi.org/10.1002/2017PA003201

Volkman, J. K., Eglinton, G., Corner, E. D. S., & Sargent, J. R. (1980). Novel unsaturated straight-chain C_{37}-C_{39} methyl and ethyl ketones in marine sediments and a coccolithophore *Emiliania huxleyi*. *Physics and Chemistry of the Earth*, *12*, 219–227. https://doi.org/10.1016/0079-1946(79)90106-X

Warden, L., van der Meer, M. T. J., Moros, M., & Sinninghe Damsté, J. S. (2016). Sedimentary alkenone distributions reflect salinity changes in the Baltic Sea over the Holocene. *Organic Geochemistry*, *102*, 30–44. https://doi.org/10.1016/j.orggeochem.2016.09.007

Weiss, G. M., de Bar, M. W., Stolwijk, D., Sinninghe Damsté, J. S., Schouten, S., & van der Meer, M. T. J. (2019). Paleosensitivity of hydrogen isotope ratios of long-chain alkenones to salinity changes at the Chile Margin. *Paleoceanography*, *34*(6), 978–989. https://doi.org/10.1029/2019PA003591

Weiss, G. M., Pfannerstill, E. Y., Schouten, S., Sinninghe Damsté, J. S., & van der Meer, M. T. J. (2017). Effects of alkalinity and salinity at low and high light intensity on hydrogen isotope fractionation of long-chain alkenones produced by *Emiliania huxleyi*. *Biogeosciences*, *14*, 5693–5704. https://doi.org/10.5194/bg-14-5693-2017

Weiss, G. M., Schouten, S., Sinninghe Damsté, J. S., & van der Meer, M. T. J. (2019). Constraining the application of hydrogen isotopoic composition of alkenones as a salinity proxy using marine surface sediments. *Geochimica et Cosmochimica Acta*, *250*, 34–48. https://doi.org/10.1016/j.gca.2019.01.038

Wolhowe, M. D., Prahl, F. G., Probert, I., & Maldonado, M. (2009). Growth phase dependent hydrogen isotopic fractionation in alkenone-producing haptophytes. *Biogeosciences*, *6*, 1681–1694. https://doi.org/10.5194/bg-6-1681-2009

Xu, L., Reddy, C. M., Farrington, J. W., Frysinger, G. S., Gaines, R. B., Johnson, C. G., et al. (2001). Identification of a novel alkenone in Black Sea sediments. *Organic Geochemistry*, *32*(5), 633–645. https://doi.org/10.1016/S0146-6380(01)00019-5

Zheng, Y., Dillon, J. T., Zhang, Y., & Huang, Y. (2016). Discovery of alkenones with variable methylene-interrupted double bonds: Implications for the biosynthetic pathway. *Journal of Phychology*, *52*, 1037–1050. https://doi.org/10.1111/jpy.12461

Zheng, Y., Huang, Y., Andersen, R. A., & Amaral-Zettler, L. A. (2016). Excluding the di-unsaturated alkenone in the U^K_{37} index strengthens temperature correlation for the common lacustrine and brackish-water haptophytes. *Geochimica et Cosmochimica Acta*, *175*, 36–46. https://doi.org/10.1016/j.gca.2015.11.024

Ziegler, M., Jilbert, T., de Lange, G. J., Lourens, L. J., & Reichart, G. J. (2008). Bromine counts from XRF scanning as an estimate of the marine organic carbon content of sediment cores. *Geochemistry, Geophysics, Geosystems*, *9*(5). https://doi.org/10.1029/2007GC001932

Zweng, M. M, Reagan, J. R., Antonov, J. I., Locarnini, R. A., Mishonov, A. V., Boyer, T. P., Garcia, H. E., Baranova, O. K., Johnson, D. R., Seidov, D., & Biddle, M. M. (2013). *World Ocean Atlas 2013, Volume 2: Salinity*. S. Levitus & A. Mishonov (Eds.). *Technical Ed.* (pp. 39). Silver Spring, MD: NOAA Altas NESDIS 74.